Minimal functional alignment of ventromedial prefrontal cortex intracranial EEG signals during naturalistic viewing

Tiankang Xie[1]
Jin Hyun Cheong[1]
Jeremy R. Manning[1]
Amanda M. Brandt[1]
Joshua P. Aronson[2]
Barbara C. Jobst[2]
Krzysztof A. Bujarski[2]
Luke J. Chang[1,*]

[1]Dartmouth College
Hanover, NH 03755
[2]Dartmouth-Hitchcock Medical Center
Lebanon, NH 03756

[*]Corresponding Author: luke.j.chang@dartmouth.edu

Word Count: 5,171

Keywords: intracranial stereo EEG, inter-subject correlation, shared response model, ventromedial prefrontal cortex, naturalistic, affect

Abstract

The ventromedial prefrontal cortex (vmPFC) has been thought to play an important role in processing endogenous information such as generating subjective affective meaning. Unlike sensory cortex, which processes exogenous information about the external world similarly across individuals, prior work has posited that vmPFC activity may be idiosyncratic to each individual, even when exposed to the same external stimulus. In this study, we recorded local field potentials (LFPs) from intracranial stereo electrodes implanted in patients with intractable epilepsy while they watched an emotionally engaging television show episode and evaluated temporal synchronization of these signals across participants in auditory cortex and vmPFC. Overall, we observed markedly lower intersubject synchronization of signals recorded from electrodes implanted in vmPFC compared to auditory cortex. A subset of patients, however, appeared to share similar vmPFC states during the more emotionally salient scenes. This work suggests that the vmPFC is involved in processing affective responses to ongoing experience in a state-like manner, but the specific states and temporal sequences are idiosyncratic to each individual, even when viewing the same television episode.

Introduction

The ventromedial prefrontal cortex (vmPFC) is a functionally heterogeneous cortical region [1,2] that has been the subject of extensive investigation over the past few decades. It is metabolically active in the absence of any explicit task [3] and coactivates with a distinct functional network that includes the posterior cingulate cortex [4,5]. The vmPFC plays a central role in learning, memory, and decision-making by facilitating the integration multimodal value signals [6–11], representing latent contextual information [12–14], and remembering the past and projecting into the future [15]. The vmPFC also processes affective and social information by generating [16–19] and regulating affective states [20–23], and by supporting internally generated self-referential thought [24–27]. Because the vmPFC is anatomically connected to many systems involved in processing affective and conceptual information including the brainstem, insula, medial temporal lobe, and prefrontal cortex, it has been hypothesized to be the hub in generating affective meaning [28–31]. However, generating affective meaning is a highly idiosyncratic process that synthesizes endogenous signals that are unlikely to be common across participants, even when they are exposed to the same exogenous stimuli or experiences.

Unlike unimodal cortex that processes exogenous information about the external world, the vmPFC is at the pinnacle of transmodal association cortex that processes endogenous information pertaining to our past experiences, current homeostatic states, and future goals [32–35]. Consequently, responses in this region are highly variable across individuals, exhibiting little evidence of intersubject spatiotemporal synchronization across a variety of experimental contexts such as listening to stories [36], watching movies [31,37,38], multivariate decoding [39], or functional connectivity patterns in resting state fMRI [40,41]. For example, in a recent fMRI study, in which participants watched a pilot episode from a character-driven television drama, we observed minimal amounts of intersubject synchronization in the vmPFC compared to unimodal sensory cortex [31]. Instead, participants appeared to dynamically switch between a few discrete states while watching the show. Though the vmPFC states were spatially consistent across participants, they were experienced at different times for each participant, with the largest temporal synchronization of states occurring at the most emotionally salient moments in the episode. Using these spatial patterns as indicators of an endogenous state revealed consistent activations distributed throughout the brain in distinct affective networks despite not being consistently time-locked to the external stimuli. While this study demonstrated a clear dissociation between how exogenous and endogenous information are processed in the brain, there are a number of open questions that remain unanswered. First, though the primary results were replicated across two independent fMRI datasets, it is unclear how much the effects might simply reflect artifacts of the BOLD fMRI signal itself. For example, the vmPFC is notoriously difficult to image due to its close proximity to the orbital sinus, which creates susceptibility artifacts in the magnetic field resulting in large signal dropout and spatial distortion [42,43]. Second, the BOLD signal reflects a downstream process of neural firing, and heterogeneity in individual vascular systems may lead to individual variations in hemodynamic responses [44–46].

To address these limitations, we sought to more directly assess temporal synchronization of vmPFC activity using intracranial electrophysiological recordings of local field potentials (LFPs). Unlike fMRI, intracranial recordings do not suffer from susceptibility artifacts, and can measure

signals with high temporal resolution from very specific spatial locations. Prior intracranial work investigating the vmPFC has relied on more traditional task-based paradigms to characterize its role in computing value [47–50]. Stimulation paradigms have implicated the involvement of the vmPFC in the subjective experience of affect, olfaction, and gustation [51,52]. Naturalistic designs, such as passive movie watching, can provide rich contextual information, which makes them well suited for studying social, cognitive, and affective processes [53–55], but have been rarely used in intracranial EEG research [56,57]. The majority of work using naturalistic designs has instead focused on characterizing sensory processes in auditory cortex and found that power in high frequency bands, such as gamma (γ), positively correlate with the envelope of the auditory stimulus [57] and also with fluctuations in the BOLD response in auditory cortex of other participants viewing the same stimulus while undergoing fMRI [56]. Power in low frequency bands, in contrast, exhibits an inverse relationship and negatively correlates with auditory signals and fluctuations in BOLD.

In the present study, we recorded intracranial stereo electroencephalogram (sEEG) data from 14 patients undergoing surgical intervention for intractable epilepsy while they viewed a 45-minute television episode (*Friday Night Lights)*. We were primarily interested in evaluating the temporal consistency of responses in the vmPFC across patients compared to the auditory cortex. Intersubject correlation analysis (ISC; [37,58] has emerged as the predominant method to evaluate the functional alignment of signals across participants. High levels of ISC indicate that participants are processing information pertaining to the stimuli similarly, while low ISC indicates high intersubject heterogeneity. However, there are several difficulties to evaluating this question in this patient population. First, both the number and location of implanted sEEG electrodes are determined by clinical needs rather than research interests, which results in only a small fraction of the cerebral cortex being covered by any given patient's electrodes, along with little overlap in implantation locations across patients. This differences in electrode numbers and locations makes across-subject comparison difficult [59]. Second, electrodes implanted in the same participant and recorded from the same shaft are not entirely independent, and are likely to be reflecting similar signals. Failure to account for the subject clustering effects and electrode distances can bias the ISC metric. To address these limitations, we assess the impact of within subject similarity and spatial distance on ISC in the vmPFC and auditory cortex and evaluate the ability of functional alignment [60,61] to overcome these inherent challenges to working with sEEG data.

Results

Inter-electrode temporal synchrony

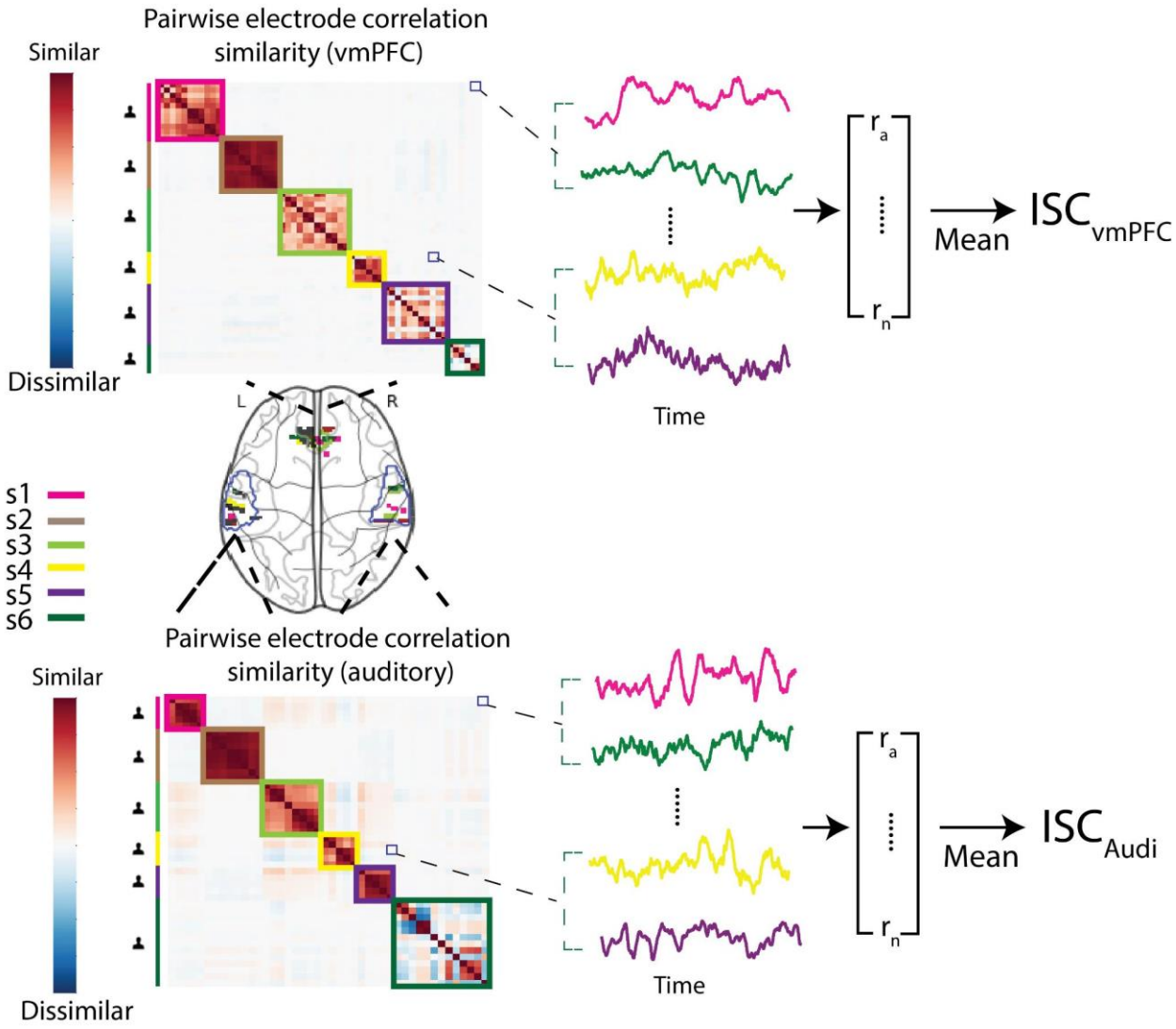

Figure 1. Electrode locations and temporal similarity. *Here we illustrate the electrode locations within the vmPFC and bilateral auditory regions of interest. Electrode anatomical locations vary across subjects. We compute the pairwise correlations between electrodes. The similarity of electrode pairs recorded from within the same participants is considerably higher than across participants. Intersubject Correlation (ISC) is the mean of the lower triangle of this pairwise correlation matrix after performing a Fisher r to z transformation.*

To assess the overall synchronization levels across electrodes, we computed the temporal intersubject correlation (ISC) of broadband power for all electrodes across participants separately for the vmPFC and auditory cortex. Electrode assignment to each region of interest (ROI) was based on broad areas of cortex functionally defined by the Neurosynth meta analytic database [62] and can be viewed on neurovault (https://neurovault.org/collections/9709/). Broadband signals [63] in both the bilateral auditory cortex and vmPFC displayed significantly high ISC using an electrode-wise bootstrapping procedure [64]: auditory r=0.16, p<0.001; vmPFC r=0.15, p<0.001). We found no reliable differences in the strength of ISC between auditory cortex and vmPFC (sign permutation test, p = 0.19) (Fig. 2B). We also compared auditory cortex versus vmPFC ISC across multiple narrow frequency bands (i.e., δ, θ, α, β, and broadband γ), but did not observe any

significant differences between auditory and vmPFC ISC within any specific frequency band (Fig. S1).

This approach, however, suffers from two fundamental problems. First, the inter-electrode temporal synchrony similarity matrix includes two distinct sources of variance: intra-subject and inter-subject similarity. Because electrodes within the same participant are primarily located on the same stereotactic strip, we observed higher levels of temporal synchrony for electrodes located within participant's auditory cortex ($r=0.54$, $p<0.001$) and vmPFC ($r=0.54$, $p<0.001$), than across participants (auditory $r=0.02$, $p<0.001$; vmpfc $r=0.007$, $p<0.001$). Second, electrodes within each region are not always located in close spatial proximity, which is likely to decrease synchrony as a function of spatial distance.

To estimate and quantify the influence of spatial distance and within-subject clustering on inter-electrode similarity, we fit a linear distance regression model separately to vmPFC and auditory electrodes. Specifically, we predicted the pairwise inter-electrode broadband power temporal similarity matrix from a linear combination of the inter-electrode spatial distance and dummy variables indicating which pairs of electrodes belonged to each of the 6 participants (Fig. 2A). This analysis allows us to quantitatively model the independent effects of spatial distance and within-subject effects on inter-electrode similarity. In vmPFC electrodes, we found that both spatial distance (beta=-0.002, SE=0.0002, $t(1532) = -7.71$, $p<0.001$, $r^2=0.014$), and within-subject effects (average beta=0.618, all ps < 0.001, $F(1532) = 2148.30$, $p<0.001$, $r^2=0.986$) independently explained a substantial portion of inter-electrode similarity variance. Similarly, for auditory electrodes we found that spatial distance (beta=-0.003, SE=0.0005, $t(939)=-6.24$ $p<0.001$, $r^2=0.098$) and within-subject effects (average beta=0.83, all ps < 0.001, $F(939) = 886.79$, $p<0.001$, $r^2=0.90$) significantly accounted for temporal synchrony variance (Fig. 2D).

These linear distance regression models allowed us to quantitatively remove this nuisance variance from the pairwise temporal similarity matrix. We computed ISC on the residuals after removing the effects of spatial distance and within-subject effects and observed higher levels of residual inter-electrode temporal synchrony in auditory cortex ($r=0.015$, bootstrap $p<0.001$) compared with vmPFC ($r=0.004$, bootstrap $p=0.08$) using a sign permutation test ($p=0.01$; Fig. 2C). We also examined these effects across multiple frequency bands and consistently found low ISC values in vmPFC across frequency bands (Fig. S2).

Taken together, these results indicate that within both vmPFC and auditory cortex, broadband temporal dynamics were more similar across electrodes within the same participant than across participants, and that nearby electrodes exhibited more similar broadband temporal dynamics than distance electrodes. After conditioning on both of these effects, we found that electrodes within the auditory cortex exhibited significantly higher levels of broadband temporal synchronization across subjects than electrodes within vmPFC.

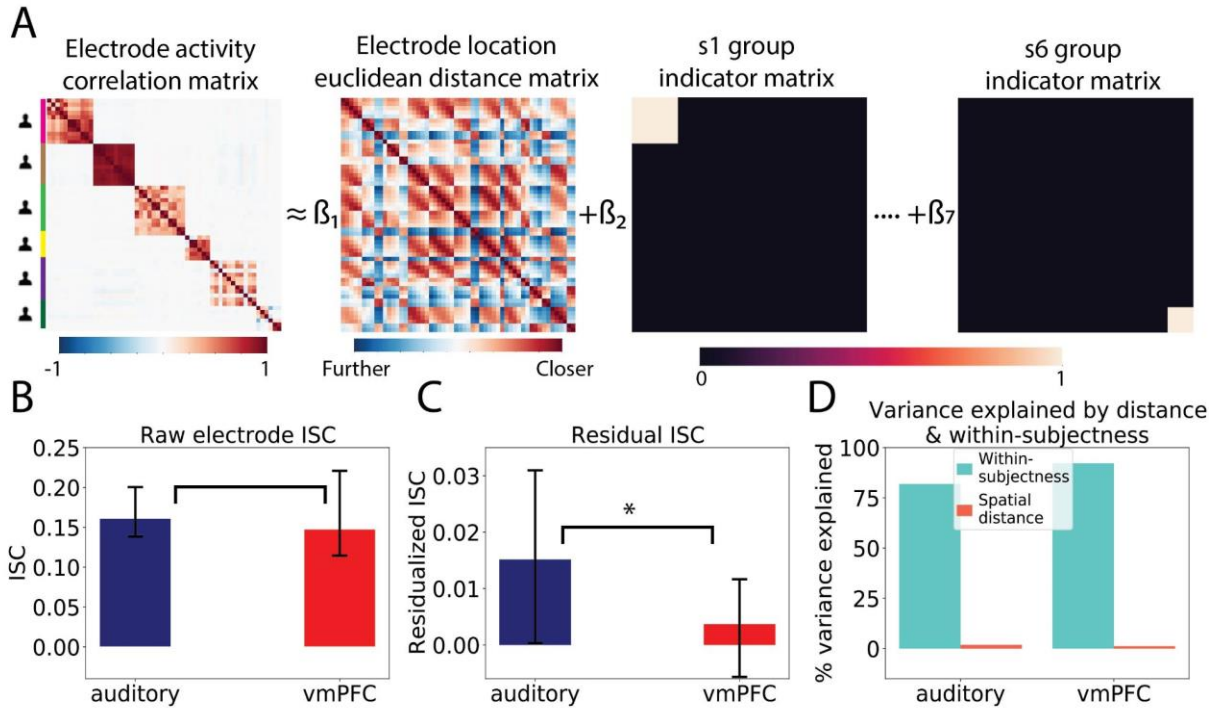

Fig. 2. Temporal Synchrony Distance Regression. *A. We used a fixed-effects regression to separate out the effect of spatial locations and within-subject clustering on pairwise electrode temporal distance. B. We observed high temporal synchronization of broadband power in both vmPFC and auditory electrodes. The auditory broadband ISC is not statistically different from the vmPFC broadband ISC (sign permutation test, p = 0.19). C. After removing within-subject clustering and spatial distance effects, we see a marked decrease in temporal ISC in vmPFC, but not auditory cortex. Now the auditory broadband ISC is significantly higher than vmPFC (sign permutation test, p=0.01) D. Overall percentage of variance explained by spatial distance and within-subject clustering in auditory/vmpfc regression model (i.e., r^2). Although both explain a significant amount of variance, the within clustering effect explains the majority of variance in the pairwise correlation values. Error bars indicate 95% confidence interval for the ISC values (See details in Method section).*

Improving inter-electrode alignment with the Shared Response Model

Our distance regression approach allowed us to estimate the impact of spatial distance and the subject-specific correlation pattern for each participant (Fig. 1, diagonal blocks). However, these regressions are based on the assumptions that: (a) millimeter-scale discrepancies in spatial location correspond to linear changes in temporal synchrony within each region, and (b) each electrode is statistically independent of the other electrodes. Although these simplifying assumptions enabled us to gain the new insights summarized above, we also know from prior work that neither of these assumptions are likely to be (strictly) true. To address these issues, we evaluated the efficacy of aligning the electrodes across participants within each region to a common latent space using the Shared Response Model (SRM; [60].

SRM was originally developed to perform functional alignment [61,65] on fMRI data by remapping voxels into a common latent space based on shared responses to time-synchronized stimuli [60,66]. This mapping is learned using a data-driven unsupervised latent factor algorithm. Formally, for

each subject i's number-of-electrodes by number-of-timepoints data matrix, X_i, SRM finds an individual basis W_i, and a latent time series matrix S, subject to the constraint that S is common across all participants. This allows X_i to be approximated by $X_i = W_i S + E_i$, where W_i and E_i are subject-specific and where S is the latent embedding shared across all m participants (Fig. 3). Here, we use SRM to align electrodes within the auditory or vmPFC regions, based on putative shared temporal dynamics across participants.

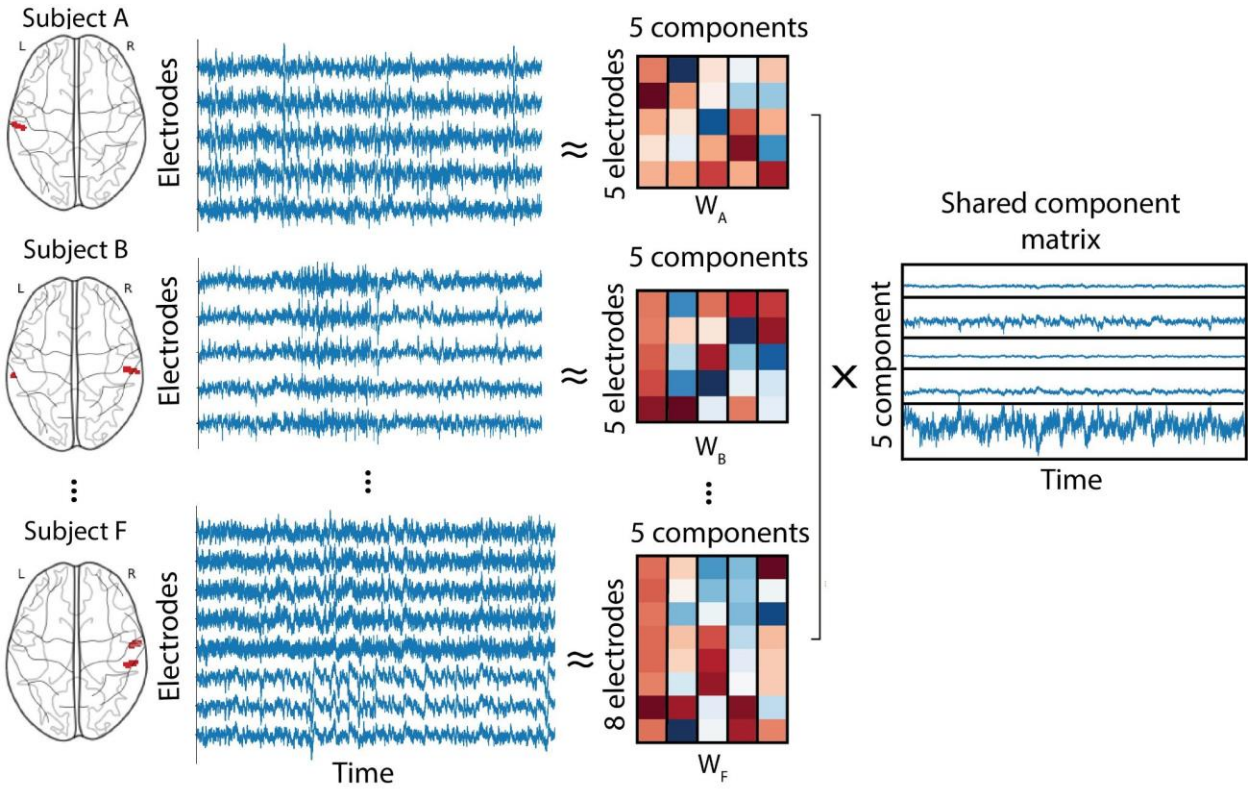

Fig. 3. Shared Response Model. *Graphical depiction of Shared Response Model applied to auditory electrodes. We applied SRM to electrodes in 6 subjects and decomposed electrode voltage in each subject into subject-specific basis functions that project into a shared component matrix common across all subjects.*

We first attempted to validate how well this technique performs in functionally aligning the sEEG electrodes. We hypothesized that aligning electrodes within the auditory cortex should result in a signal that directly corresponds to properties of the auditory stimulus while participants watched the show. For example, prior work has shown that lower frequency power tends to negatively correlate with the audio envelope of auditory stimuli, whereas higher frequency power tends to positively correlate with the auditory signal [56,57,67]. To test this hypothesis, we estimated a 5-dimensional SRM using the band-pass filtered voltage activities of 44 auditory electrodes from 6 subjects. We selected the SRM component with the highest ISC across subjects (ISC = 0.04, $p<0.001$) and computed the time-varying power in the low δ (i.e., 1-2 Hz) and high γ (i.e., 70-150 Hz) power bands. We then correlated these signals with the raw audio envelope to assess how well this approach was able to recover the true signal we expected to be present in the data (Fig. 4A). Consistent with prior work [56,57], we found that power in the δ band negatively correlated with

the audio envelope (r=-0.22, p<0.001), while the broadband γ power of the SRM component positively correlated with the raw audio envelope (r=0.06, p<0.001). We also found that the SRM component exhibited a tighter coupling of the audio envelope in both δ and high γ frequency bands compared to simply averaging power from electrodes across participants (low delta: $p < 0.001$; broadband gamma: $p = 0.02$). This analysis indicates that the SRM can extract meaningful functional signals from a well-characterized region of cortex, and that SRM outperforms simple across-participant electrode averaging.

We next explored the impact of the SRM transformation on the power spectral density (PSD). EEG LFPs tend to reflect higher power in lower frequency components (the well characterized 1/f noise) and this may have impacted the functional alignment procedure. We computed the mean-normalized power spectrum density (PSD) of the maximum SRM component and compared this to the PSD of the average electrode bandpass filtered voltages. Overall, we found that the SRM component did not appear to substantially alter the PSD in either auditory cortex or vmPFC (Fig. 4B).

Another potential benefit of applying SRM to LFPs relates to artifact removal. Because SRM attempts to temporally align signals that are shared across participants, it likely implicitly removes artifacts that are not time-locked across participants. For example, removing ictal activity and interictal epileptiform discharges (IEDs) is well-known in the intracranial literature to present a substantial computational challenge [68,69]. Several factors, including lack of precise and established definitions of epileptic spikes and wide spectrum of morphologies of epileptiform abnormalities both within the same patient and across patients, contribute to the difficulties in identifying and removal of IEDs [70–72]. However, because IED morphologies are unique to each participant and occur at different times, we hypothesized that SRM should be effective in removing these idiosyncratic signals. Indeed, we found that SRM was able to successfully remove IEDs and Ictal activities (Fig. 4C). In addition, SRM was able to reduce the impact of 60Hz power line noise by an average of 51% (Fig. S3; see supplementary materials for details).

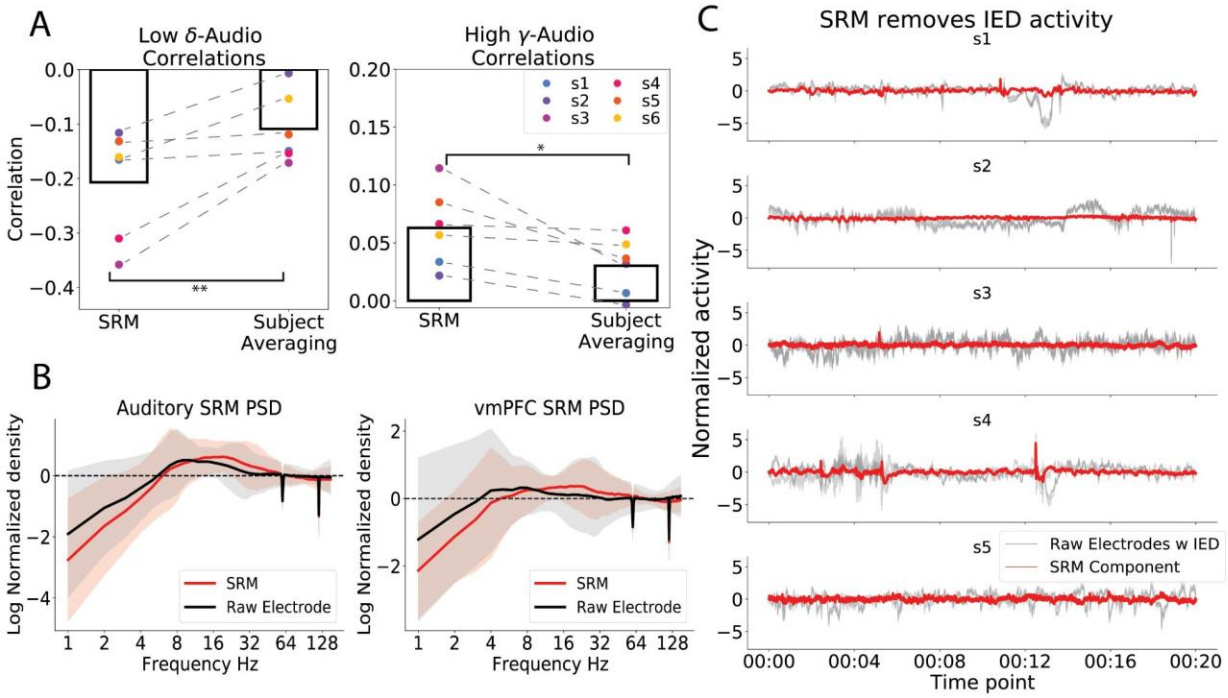

Fig. 4. Validating SRM on auditory cortex. *A: SRM component from auditory cortex electrodes better captures the audio-specific stimuli than the subject-averaging method. Left: correlation between SRM low δ power (1-2 Hz) and audio envelope; Right: correlation between SRM high γ power (70-150 Hz) and audio envelope (*: 0.01<=p<0.05; **: 0.001<p<=0.01). B: The log-log plot for Power Spectrum Density of auditory and vmPFC max SRMs. The 1/f trend is removed by fitting a first-order linear regression and obtaining the residuals. We plotted the subject-averaged and 1/f detrended PSDs for both the max SRM component (red lines) and the original electrode channels (black lines). Shaded areas indicate 95% confidence intervals. We see that the SRM does not substantially distort the original electrode PSD. C. To estimate the extent to which SRM can reduce IED and Ictal (seizure) activities, we apply SRM to 20s of selected time periods in amygdala electrodes in 5 subjects where a mixture of IEDs and Ictal activity patterns is clearly visible by eye. We apply SRM to data with IED and Ictal activities and we found that SRM removed the subject-specific IED and Ictal activities.*

vmPFC activity does not align across subjects

After validating the SRM method on the auditory cortex, we next were interested in evaluating shared signals in the vmPFC after aligning electrodes with SRM. We trained an SRM with 6 components on vmPFC electrodes and transformed each participant's observed data into the shared latent space. We selected the SRM component with the highest ISC across subjects (ISC=0.01, p=0.004). We also computed the ISC across broadband powers and several narrow band frequencies (i.e., δ, θ, α, β, and low and high γ). We did not observe a significant effect of intersubject synchronization across any frequency band (Fig. 5). To ensure that these results were completely unbiased from training and testing the SRM model on the same data, we also performed a split-half cross-validation procedure, in which we trained the model on the first or second half of the data and tested it on the other half. Overall, we observed consistent results, in which ISC was not significantly different from zero, even when the SRM model was trained on independent data (Fig. S4).

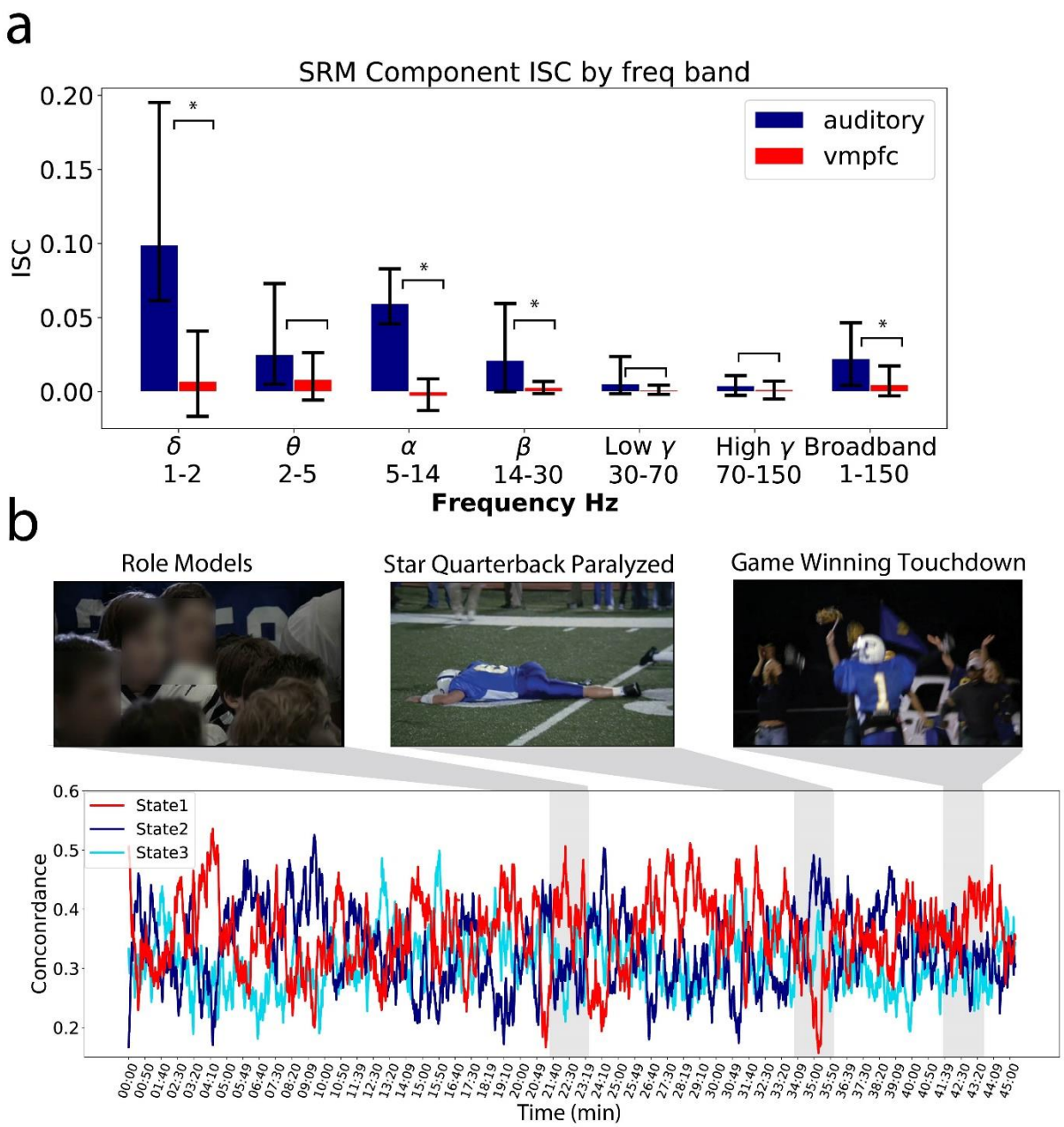

Fig. 5. Shared Response Model vmPFC Alignment. *A) Inter-subject correlation value for auditory (blue) and vmPFC (red) electrodes. After identifying the SRM component with the highest ISC across participants, we extracted power from different frequency bands and computed ISC within each band including broadband power. Error bars indicate 95% confidence interval for the ISC values (See details in Method section), * indicates p<0.05 using subject-wise bootstrapping. B) Line plots illustrate each HMM state concordance across participants at each time moment during the episode and have been smoothed with an exponential smoothing function with alpha = 0.001 for visualization. Shaded regions indicate scenes associated with intense affective experiences reported in [31]. State 1 appears corresponds to positive affective scenes while State 2 corresponds to negative affective scenes. Screenshots from Friday Night Lights are copyright of NBCUniversal, LLC.*

Temporal alignment of discrete SRM states across participants

The above ISC analyses provide converging evidence with the distance regression analyses indicating minimal evidence of consistent across-participant temporal synchronization in the vmPFC across the 45min episode. However, it is possible that there might be particular time points during which participants briefly experienced the same psychological state. For example, in a previous fMRI study, we found evidence that participants were more likely to occupy the same psychological state during scenes that elicited more intense affective experiences [31]. These states were identified directly from brain activity using Hidden Markov Models (HMMs), and were validated on self-reported time-varying feelings and facial expressions. Following our prior approach, we fit an HMM to the broadband power of the 6 SRM components separately for each individual participant. We made the following implicit assumptions: (1) the latent state transitions follow a first order Markovian Process, (2) the SRM components were modeled using an orthogonal multivariate Gaussian Distribution, and (3) all participants experienced the same number of latent states. We used the Viterbi algorithm [73] to obtain the most likely sequence of latent states for each participant. States derived from each HMM were then aligned across participants by maximizing the cross-subject state similarity using the Hungarian Algorithm [74]. We estimated the number of HMM states by computing the Bayesian Information Criterion (BIC) across a range of states ($k = [2, 15]$) and found that k=3 states exhibited the greatest improvement in model fit (Fig. S7). Finally, we computed the across-patient state concordance at each moment in time by calculating the proportion of participants occupying the same state within each time interval (Fig 5B). Higher concordance values indicate that more participants were sharing a common psychological state.

During several scenes that we identified in our prior work as having particularly high emotional salience and narrative importance [31], we found that the patients tended to converge on the same HMM states. These scenes included a positive sentimental scene when the football players provide mentorship to younger kids (~22 min, State 1), a negative scene when the the star quarterback is severely injured during a play and undergoes emergent surgery (~35 min, State 2), and a positive scene when the nervous and inexperienced backup quarterback throws a game winning pass (~42 min, State 1). Though only 50% of the patients converged on the same states during these scenes, it is notable that State 1 concordance increased during positively valenced scenes, while State 2 concordance increased during negative arousing scenes. These results are consistent with the hypothesis that the vmPFC is involved in generating affective meaning [19,29–31] and demonstrate that the minimal synchronization observed in the ISC analyses cannot be explained by the absence of any meaningful signal in the vmPFC LFPs.

Discussion

The majority of cognitive neuroscience research has focused on mapping stimulus-driven neural activity patterns that are common across participants. This approach has been highly successful in developing a deep understanding of how the brain processes exogenous information about the external world. However, this approach may have limited utility when characterizing regions that process endogenous information that may be idiosyncratic to each individual participant such as the transmodal cortex [35]. The vmPFC has been theorized to be intimately involved in generating

affective meaning by integrating stimulus-driven information with an individual's unique history of past experiences, internal homeostatic states, and future goals [29–31]. Consequently, activity in this region has been highly variable across individuals in a variety of tasks [37,39,40]. Consistent with these observations, we have previously found using fMRI that unlike unimodal sensory cortex, the vmPFC does not appear to synchronize across participants when passively viewing an emotionally engaging television drama except during particularly salient emotional scenes [31]. The vmPFC, however, is notoriously difficult to image using BOLD fMRI due to signal drop out and geometric distortions arising from susceptibility artifacts. Therefore, in this paper, we sought to examine inter-subject synchronization of vmPFC activity based on LFPs recorded using sEEG in patients undergoing surgical intervention for intractable epilepsy when watching an emotionally arousing naturalistic stimulus. Overall, our results are highly consistent with the previously reported fMRI findings. We find strong evidence of common signals being processed in the unimodal auditory cortex, but minimal evidence of cross-participant temporal synchronization in the vmPFC across any specific frequency band. However, this region does appear to reflect the idiosyncratic ways we assign affective meaning to incoming stimuli as approximately 50% of our sample appeared to be sharing a similar valenced interpretation of the most emotionally salient scenes based on our individual-HMM analysis.

A methodological challenge to evaluating shared signals across participants using sEEG is that electrodes are not located in the same spatial locations across participants. Electrode locations are determined based on clinical needs for monitoring epileptiform activity and surgical planning. For example, even though we collected data from 14 patients, only 6 had electrodes placed within both of our target regions of interest (i.e., vmPFC & auditory cortex). A major contribution of this work is the application of alignment procedures that allow signals within a region originating from different anatomical locations to be compared across participants. We used two different approaches that are novel to analyzing sEEG data. First, we performed linear distance regression to estimate and remove variance in the pairwise electrode temporal similarity matrix resulting from variations in the spatial distance of electrode placement and intra-subject covariance from electrodes located on the same stereotactic strip. Overall, we found that over 90% of the variance of the electrode temporal similarity matrix could be explained by these two different types of signals. Removing these signals revealed that processes in the auditory cortex, but not vmPFC appeared to be shared across participants. Second, we performed functional alignment using SRM. This approach attempts to align latent signals present in the electrodes based on commonality across participants and importantly can accommodate different numbers of electrodes for each participant. We demonstrate that this approach is better able to recover auditory signals in the auditory cortex compared to simply averaging electrodes. In addition, SRM can also be effective in removing many sources of noise that are idiosyncratic to each individual participant such as IEDs and Ictal activities and even power line noise to some extent. This was confirmed by selectively adding different types of noise to each participant and evaluating how much of the noise was removed by the SRM procedure. Similar to the distance regression approach, we only observed common signals in the auditory and not vmPFC cortex across participants after performing this alignment procedure. These results indicate that SRM provides a promising technique for both denoising signals, but also in functionally aligning electrodes and may complement alternative techniques such as SuperEEG [59].

Our results suggest that processes in transmodal cortex such as the vmPFC appear to be idiosyncratic to each individual and do not directly map onto processing exogenous information from the eliciting naturalistic stimulus. These results are in line with our previous fMRI findings in which two independent samples of participants watched the same video [31]. Importantly, this work confirms that the fMRI results cannot be fully attributed to signal dropout and geometric distortions in the BOLD signal arising from susceptibility artifacts in the magnetic field where tissue borders air in the orbital sinus. How then should this null result be interpreted? On the one hand, variations in LFPs in the vmPFC across participants could arise from participants engaging in stimulus-independent thought such as mind wandering [24,75]. Alternatively, participants could be making stimulus-dependent evaluations about the affective meaning of the stimulus with respect to their idiosyncratic goals, experiences, and homeostatic states [29–31]. One of the most simple appraisals an individual can make is whether they like or dislike a stimulus or event. These subjective value judgments require integrating multiple attributes of a stimulus with respect to salient goals [6,8]. For example, when appraising the value of food, the vmPFC appears to integrate multiple attributes such as taste, cost, and caloric content [11] with broader goals such as eating healthy [76] and internal homeostatic drives [77]. Thus, it seems plausible that participants may be generating their own unique appraisals about the events in the television show as they unfold. The results from our HMM analysis support this latter interpretation. We find that participants are more likely to occupy the same vmPFC state during the more emotionally evocative scenes and that distinct states appear to map onto the affective valence of the scene, providing a direct replication of our fMRI study [31]. Importantly, in these emotionally salient scenes, approximately only 50% of our sample appeared to occupy the same state. This likely explains why we did not observe synchronization using the ISC method, which would require more consistent temporal synchronization from the majority of the participants.

More broadly, this work presents a fundamental challenge to studying the computations performed by the vmPFC. The majority of cognitive neuroscience research relies on group analyses to make inferences and these findings reveal that participants do not share consistent processes when viewing a rich and engaging naturalistic stimulus. Future work will need to develop novel research paradigms and analytic frameworks that can account for this intersubject heterogeneity to better characterize the computations performed by this region of cortex. Several promising approaches include the idiographic approach employed in studies of valuation [6] and aesthetic experiences [78], intersubject representational similarity analysis [79–81], and fitting HMMs directly to single subject brain activity [31].

There are several potential limitations of this work that are important to highlight. First, it is unknown to what extent these results may be attributed to the pathophysiology of epilepsy or its pharmacological treatment. Both chronic refractory epilepsy and antiepileptic drugs could have a profound effect on the patient's brain responses and cognitive functions [82–86]. However, we presume that these results will generalize beyond the specific participants and patient populations included in our analyses. Second, our analyses assume that our sampled electrodes in the vmPFC cover regions performing similar functions across participants. However, it is well known that the vmPFC is composed of several functionally separable regions [1]. Thus, it is possible that the implanted electrodes may be located in regions that are not functionally homogeneous across participants. This particular issue may be more problematic for single unit recordings, as LFPs

are likely reflecting coordinated firing of populations of neurons distributed across larger areas of cortex [67]. Third, the maximum number of components we were able to estimate for the SRM was determined by the smallest number of electrodes implanted in any participant [60]. It is highly likely that the vmPFC contains many more than 6 latent components (the fewest number of electrodes in this region in a single participant). However, we think this is unlikely to change our results as we focused specifically on the component with the highest synchronization across participants. Fourth, our HMM analysis assumes that all participants experienced the same number of states. It is highly unlikely that all subjects experienced the same number of latent states, but this simplifying assumption was necessary to enable the alignment of states and compute the state concordance across participants.

In summary, using a naturalistic paradigm with sEEG recordings, we investigated intersubject synchronization of dynamic LFP signals in the vmPFC. Overall, we found minimal evidence indicating that signals in this region are shared across participants during this experimental context after removing artifacts related to spatial distance and within subject clustering. However, our individual-HMM analysis revealed that some vmPFC states appeared to show increased alignment during emotionally salient scenes. These results are highly consistent with previous work using fMRI [31] and suggest that the vmPFC is involved in processing affective responses to ongoing experience in a state-like manner, but the specific states and temporal sequences are idiosyncratic to each individual. Beyond the vmPFC, we observed strong synchronization in the δ, α, and β bands of auditory cortex that directly mapped onto properties of the eliciting auditory stimulus. In addition, we demonstrate that SRM [60,61] can be a promising technique to aid in functionally aligning signals from electrodes implanted in different regions across participants and also in denoising sEEG data.

Methods

Participants

In this study, we recruited 14 epilepsy patients (mean age = 38.6, sd=11.7; 5 females) undergoing inpatient stereo-EEG monitoring at the Dartmouth-Hitchcock Medical Center. sEEG electrode placement is determined solely based on clinical needs and we only included participants with electrodes implanted in both vmPFC and auditory regions (n=6, mean age = 45.6, sd = 12.3, 3 females), (See table 1 for detailed information on electrodes and subjects). All participants provided informed consent approved by the Institutional Review Board at Dartmouth-Hitchcock Medical Center.

Experiment Procedure

Participants watched the first episode of the 45-minute television drama *Friday Night Lights* while undergoing stereo-EEG monitoring at their bedside. This show was selected because of its engaging and emotionally evocative content. The show was presented on a Windows computer using either PsychoPy [87] or SuperLab (Cedrus, San Pedro, CA USA). Triggers indicating the

onset and offset of the stimulus were sent to the sEEG recording system. Electrodes used in the study were either 0.86 mm diameter Ad-Tech (Ad-Tech Med Instr Corp, USA) sEEG with 10 independent recording contacts per electrode or 0.8 mm diameter PMT (PMT Corp., USA) sEEG with 8-12 independent recording contacts per electrode. Intracranial data were recorded on a Natus XLTek EMU 128 system at 2048Hz.

Channel Selection

We assigned electrodes to each region of interest (ROI) based on broad areas of cortex functionally defined by the Neurosynth meta analytic database [62]. For each electrode we created a sphere of radius 2mm centered at the electrode's MNI location. We then calculated the percentage overlap between the electrode sphere and each ROI region mask. We included electrodes with greater than 50% overlap within each ROI region mask. Electrode assignments and ROI region masks can be viewed at https://neurovault.org/collections/9709/).

Signal Preprocessing

A careful visual inspection was conducted on the collected sEEG data by a qualified neurologist to exclude all bad/corrupted electrodes or electrodes with excessive epileptic activities. sEEG data was high-pass filtered at 0.1 Hz to remove slow drifts and a 60 Hz FIR notch filter was applied to remove electrical interferences. We used Laplacian re-referencing to electrodes on each stereotactic strip to extract local population-level activity [88] and downsampled the data to 512 Hz to speed up subsequent analysis computations. Data preprocessing was performed in Python 3.7.9 with the MNE [89], Numpy [90], and Scipy [91] packages.

Time-Frequency Processing

Unless otherwise specified, we used Morlet Wavelet Transforms implemented in the MNE package (function: *tfr_array_morlet)* [89] with a width of 7 cycles for all time frequency decomposition analyses discussed in the paper. Specifically, we created 30 logarithmically spaced frequency bins ranging from 1 Hz to 150 Hz, applied the wavelets to each frequency bin, and calculated the power. Power modulations that fall between 56 - 64 Hz and 116-124 Hz are not included because of their proximity to the 60 Hz power line noises and 120 Hz harmonics. We divided the power in each frequency bin by its mean to convert the absolute power values to a proportion of the mean [92]. This normalization procedure minimizes power differences across frequency bands resulting from their 1/f distribution. Finally we averaged all power estimates for the wavelet frequency bins within δ (1-2Hz), θ (2-5 Hz), α (5-14 Hz), β (14-30 Hz), low γ (30-70 Hz), high γ (70-150 Hz), or overall broadband power (1-150Hz) bands. We also ran all time-frequency decomposition analyses with Hilbert transformation and observed similar results.

Power-Spectrum Density

We calculated the power spectrum density (PSD) of the signal using Welch's Method with a Hamming window of 1s with 50% overlap. In Fig 4B & Fig S3, we removed the 1/f power decay

by log-transforming the power and frequency bins estimated from Welch's Method, fitting a linear regression and finally plotting the residuals from the regression. We used implementations from mne-python (function: *psd_array_welch*) [89] for Welch's Method and implemented the linear regression with scikit-learn (function: *LinearRegression*) [93]

Inter-subject Correlation (ISC)

In order to measure the degree of shared information patterns across subjects, we used the *Intersubject correlation* (ISC) metric [37]. ISC is a simple yet effective way to reliably extract the shared brain responses to complex naturalistic stimuli across individuals [58]. ISC was originally developed for fMRI data analysis but has also been applied to other neuroimaging modalities such as EEG [94–98], MEG [99–101].

We applied ISC to our intracranial EEG data to study the degree of functional alignment across subjects separately within auditory and vmPFC electrodes. We calculated ISC as the mean value of the lower triangle of the pairwise correlation matrix, excluding the diagonal elements. We applied fisher's z-transform to transform the pairwise correlation value prior to taking the mean and used the inverse fisher transform to convert the mean z-transformed value back to correlation. Each correlation pair is calculated as:

$$corr(x,y) = \frac{\sum_{i=1}^{N}(x_i - \bar{x_i})(y_i - \bar{y_i})}{\sigma_x \sigma_y} \quad \text{(eq 1)}$$

where,

$$\sigma_x = \sqrt{\sum_{i=1}^{N}(x_i - \bar{x})^2} \quad \text{(eq 2)}$$

and

$$\bar{x} = \frac{1}{N}\sum_{i=1}^{N} x_i \quad \text{(eq 3)}$$

The overall ISC is thus,

$$ISC_{1,\dots N} = R(\frac{\sum_{i=1}^{N}\sum_{j=1}^{i} Z(corr(S_i, S_j))}{N(N-1)}) \quad \text{(eq 4)}$$

where,

$$Z(x) = \frac{1}{2} ln(\frac{1+x}{1-x})$$

and

$$R(x) = \frac{e^{2x}-1}{e^{2x}+1} \quad \text{(eq 5)}$$

S is the 'subject' matrix of shape either number of electrodes by time (for raw electrode & residualized analysis, N=44) or number of subjects by time (for the subsequent SRM analysis, N=6).

To test if ISC values are significantly above zero, we used subject-wise bootstrapping as recommended by [64]. Specifically, we sample the pairwise correlations in the lower triangle correlation matrix with replacement and calculate the ISC after removing correlations between the same electrode. We repeated the process 5000 times and calculated the p-value for our two-tailed hypothesis test.

We used the ISC and bootstrap implementations from our python analysis package nltools [102] available at https://nltools.org/.

Distance Regression

To perform our distance regression (Fig. 2A), we first computed the pairwise correlation matrix separately for vmPFC or auditory electrodes across 6 subjects. Next, we calculated a pairwise Euclidean Distance matrix using the x/y/z millimeter MNI coordinates separately for vmPFC or auditory electrodes across 6 subjects. Prior to running the regression, we Fisher z-transformed the correlation matrix and centered the distance matrix by subtracting its grand mean. We then added within-subject dummy matrices for each subject, in which electrode pairs clustered within a subject were indicated by a value of 1, and 0 everywhere else. We estimated a separate linear model for each region of interest (e.g., vmPFC or auditory cortex) using the pairwise correlation matrix as the response variable and the euclidean distance matrix and 6 dummy matrices as explanatory variables using the function 'lm' in R [103]. We did not include a global intercept for the regression. The residuals of the model are obtained and used in subsequent ISC analyses. We calculated the variance explained using a nested model comparison approach where we compared the total variance explained to a subset of the model omitting either the spatial distance or the within-subject clustering dummy indicator matrices.

Shared Response Model

We performed functional alignment [61] using the Shared Response Model (SRM; [60]) separately on auditory and vmPFC electrodes across 6 subjects. As demonstrated in Fig. 4, SRM is a matrix factorization model that decomposes the electrode-by-time matrix for each subject into a common shared component matrix and an orthogonal subject-specific basis matrix. The objective function is to minimize the reconstruction loss across all 6 subjects. SRM identifies common activity patterns that are present across subjects and provides a method to transform the original electrode activities into a shared latent component space. The number of features k in our study is chosen as the minimum number of electrodes present in any given participant (k=5 for auditory, k=6 for vmPFC).

For each subject's electrodes activity matrix X_i, i=1..6, of shape (n_i, t) where n_i is the number of electrodes present in the subject (see Table S1) and t is the time length of the sEEG recording (~45 minutes), we decompose $X_i \approx W_i S$, where W_i is the orthogonal subject-specific basis function of shape (n_i, k) satisfying $W_i W_i^T = I_k$ and S is the shared components matrix of shape (k, t). The objective function is thus to minimize the squared reconstruction loss as

$min_{W_i,S} \sum_{i=1}^{6} ||X_i - W_i S||_F^2$, where $||.||_F$ is the frobenius norm. (see details in [104] about how to computationally derive a solution to the objective function). After we have identified the W_i for each subject and S for all subjects, we can use the subject's reconstructed activity matrix $X_i' = W_i S$, of shape (k, t), to approximate the subject's raw electrode activity matrix X_i. For each component $m = 1..k$, we selected the $m - th$ row (which leads to a matrix of shape $(1, t)$ for each subject) of the reconstructed matrix X_i' across 6 subjects and calculated the ISC. We selected the component m that yields the maximum ISC across 6 subjects. We used a modified version of the original Brainiak version of SRM implemented in our nltools package [102].

Statistical Tests

All hypothesis tests comparing regions used non-parametric sign permutation tests. In order to test the significance of differences between auditory and vmPFC ISC values, we randomly shuffled the group assignment of each pairwise correlation and calculated the ISC differences for the re-shuffled pairwise correlations. We repeated the process 5000 times to generate a null distribution and calculated p-values for our two-tailed hypothesis test, by counting the number of iterations that our observed difference exceeded the null distribution. For one-sample tests, we randomly multiplied each value by [1,-1] and generated a null distribution using 5000 iterations.

Extracting audio power envelope

We extracted the power envelope of the auditory stimulus using a similar procedure as [57]. We extracted power from the auditory channel using multi-tapering where power is estimated every 200 Hz from 200 Hz to 5000 Hz (25 frequency bands in total) with 3 tapers. We took the logarithm of each frequency band and further z-score normalized the power in each frequency band. Finally we averaged the powers across 25 frequency bands to get the final power envelope for the audio stimuli.

Hidden Markov Model

Hidden Markov Models are generative probabilistic state-space models which assume that the current sequence of observations is generated by a sequence of discrete latent state variables. The transitions between latent states are assumed to follow the first order Markov Process, where the probability of transition to the next immediate state depends only on the most recent state. We have also made the implicit assumption that the observed variables follow a multivariate Gaussian distribution with diagonal covariance matrix.

We fit an individual HMM separately on each participant's broadband power SRM components. Specifically we first applied a 6-component SRM to the raw vmPFC electrodes across 6 subjects, and obtained the resulting transformed matrix of shape $(6, t)$ for each subject. We extracted the broadband power from the SRM components for each participant and normalized the power for each SRM component for each participant. We fit an HMM to the normalized power matrix for each subject using the *hmmlearn Package* (version 0.2.5). We used the Viterbi algorithm to

maximize a posteriori probability estimates and infer the most likely sequence of latent states. Model parameters were estimated with expectation-maximization. In order to determine the number of states *k* for our HMM model, we calculated the Bayesian Information Criterion (BIC) value over a range of $k = [2, 15]$. BIC finds the simplest model to fit the data by balancing the maximum likelihood function and the model parameters & number of data points.

Specifically BIC is calculated as:

$$BIC = ln(n)(k^2 + 2kf - 1) - 2ln(\hat{L}) \quad \text{(eq 7)}$$

where n is the number of observations, k is the number of parameters in the model, f is the number of features (which equals to 6 SRM components in our case), and $\hat{L}$ is the maximum log-likelihood of the HMM model fit. We calculated the BIC value for each chosen $k = [2, 15]$ for each participant. For each state we averaged the BIC across 6 participants. We then selected the k which gives the maximum reduction in BIC value (i.e., the derivative of the BIC with respect to k; Fig. S7). For each fitted model, we aligned the latent states across participants by maximizing the correlation similarity between the model pairs using the Hungarian Algorithm [74].

Code

All code used to perform these analyses are available on Github https://github.com/cosanlab/naturalistic_iEEG_func_align/.

Acknowledgments

This work was supported by awards from the National Institute of Mental Health R01MH116026 and R56MH080716 to LJC. TKX is supported by the Big Data in the Life Sciences Training Program by Burroughs-Wellcome Fund.

Competing Interests

The authors declare no competing interests.

References

1. Kahnt, T., Chang, L. J., Park, S. Q., Heinzle, J. & Haynes, J.-D. Connectivity-based parcellation of the human orbitofrontal cortex. *J. Neurosci.* **32**, 6240–6250 (2012).
2. de la Vega, A., Chang, L. J., Banich, M. T., Wager, T. D. & Yarkoni, T. Large-Scale Meta-Analysis of Human Medial Frontal Cortex Reveals Tripartite Functional Organization. *J. Neurosci.* **36**, 6553–6562 (2016).
3. Raichle, M. E. *et al.* A default mode of brain function. *Proc. Natl. Acad. Sci. U. S. A.* **98**, 676–682 (2001).
4. Fox, M. D. & Raichle, M. E. Spontaneous fluctuations in brain activity observed with functional magnetic resonance imaging. *Nat. Rev. Neurosci.* **8**, 700–711 (2007).
5. Buckner, R. L. & DiNicola, L. M. The brain's default network: updated anatomy, physiology and evolving insights. *Nat. Rev. Neurosci.* **20**, 593–608 (2019).
6. Rangel, A., Camerer, C. & Montague, P. R. A framework for studying the neurobiology of value-based decision making. *Nat. Rev. Neurosci.* **9**, 545–556 (2008).
7. Hare, T. A., O'Doherty, J., Camerer, C. F., Schultz, W. & Rangel, A. Dissociating the role of the orbitofrontal cortex and the striatum in the computation of goal values and prediction errors. *J. Neurosci.* **28**, 5623–5630 (2008).
8. Padoa-Schioppa, C. & Assad, J. A. Neurons in the orbitofrontal cortex encode economic value. *Nature* **441**, 223–226 (2006).
9. Bartra, O., McGuire, J. T. & Kable, J. W. The valuation system: a coordinate-based meta-analysis of BOLD fMRI experiments examining neural correlates of subjective value. *Neuroimage* **76**, 412–427 (2013).
10. Knutson, B., Fong, G. W., Adams, C. M., Varner, J. L. & Hommer, D. Dissociation of reward anticipation and outcome with event-related fMRI. *Neuroreport* **12**, 3683–3687 (2001).
11. Suzuki, S., Cross, L. & O'Doherty, J. P. Elucidating the underlying components of food valuation in the human orbitofrontal cortex. *Nat. Neurosci.* **20**, 1780–1786 (2017).
12. Niv, Y. Learning task-state representations. *Nat. Neurosci.* **22**, 1544–1553 (2019).
13. Constantinescu, A. O., O'Reilly, J. X. & Behrens, T. E. J. Organizing conceptual knowledge in humans with a gridlike code. *Science* **352**, 1464–1468 (2016).
14. Schuck, N. W., Cai, M. B., Wilson, R. C. & Niv, Y. Human Orbitofrontal Cortex Represents a Cognitive Map of State Space. *Neuron* **91**, 1402–1412 (2016).
15. Buckner, R. L. & Carroll, D. C. Self-projection and the brain. *Trends Cogn. Sci.* **11**, 49–57 (2007).
16. Damasio, A. R. *et al.* Subcortical and cortical brain activity during the feeling of self-generated emotions. *Nat. Neurosci.* **3**, 1049–1056 (2000).
17. Eisenbarth, H., Chang, L. J. & Wager, T. D. Multivariate Brain Prediction of Heart Rate and Skin Conductance Responses to Social Threat. *J. Neurosci.* **36**, 11987–11998 (2016).
18. Lindquist, K. A., Wager, T. D., Kober, H., Bliss-Moreau, E. & Barrett, L. F. The brain basis of emotion: a meta-analytic review. *Behav. Brain Sci.* **35**, 121–143 (2012).
19. Chikazoe, J., Lee, D. H., Kriegeskorte, N. & Anderson, A. K. Population coding of affect across stimuli, modalities and individuals. *Nat. Neurosci.* **17**, 1114–1122 (2014).
20. Phelps, E. A., Delgado, M. R., Nearing, K. I. & LeDoux, J. E. Extinction learning in humans: role of the amygdala and vmPFC. *Neuron* **43**, 897–905 (2004).
21. Etkin, A., Büchel, C. & Gross, J. J. The neural bases of emotion regulation. *Nat. Rev. Neurosci.* **16**, 693–700 (2015).
22. Ochsner, K. N., Bunge, S. A., Gross, J. J. & Gabrieli, J. D. E. Rethinking feelings: an FMRI study of the cognitive regulation of emotion. *J. Cogn. Neurosci.* **14**, 1215–1229 (2002).
23. Wager, T. D. *et al.* Placebo-induced changes in FMRI in the anticipation and experience of pain. *Science* **303**, 1162–1167 (2004).
24. Mason, M. F. *et al.* Wandering minds: the default network and stimulus-independent

thought. *Science* **315**, 393–395 (2007).
25. Andrews-Hanna, J. R., Smallwood, J. & Spreng, R. N. The default network and self-generated thought: component processes, dynamic control, and clinical relevance. *Ann. N. Y. Acad. Sci.* **1316**, 29–52 (2014).
26. Kelley, W. M. *et al.* Finding the self? An event-related fMRI study. *J. Cogn. Neurosci.* **14**, 785–794 (2002).
27. Mitchell, J. P., Heatherton, T. F. & Macrae, C. N. Distinct neural systems subserve person and object knowledge. *Proc. Natl. Acad. Sci. U. S. A.* **99**, 15238–15243 (2002).
28. Damasio, A. R. *Descartes' error*. (Random House, 2006).
29. Roy, M., Shohamy, D. & Wager, T. D. Ventromedial prefrontal-subcortical systems and the generation of affective meaning. *Trends Cogn. Sci.* **16**, 147–156 (2012).
30. Ashar, Y. K., Chang, L. J. & Wager, T. D. Brain Mechanisms of the Placebo Effect: An Affective Appraisal Account. *Annu. Rev. Clin. Psychol.* **13**, 73–98 (2017).
31. Chang, L. J. *et al.* Endogenous variation in ventromedial prefrontal cortex state dynamics during naturalistic viewing reflects affective experience. *Sci Adv* **7**, (2021).
32. Margulies, D. S. *et al.* Situating the default-mode network along a principal gradient of macroscale cortical organization. *Proc. Natl. Acad. Sci. U. S. A.* **113**, 12574–12579 (2016).
33. Paquola, C. *et al.* Microstructural and functional gradients are increasingly dissociated in transmodal cortices. *PLoS Biol.* **17**, e3000284 (2019).
34. Margulies, D. S. & Smallwood, J. Converging evidence for the role of transmodal cortex in cognition. *Proceedings of the National Academy of Sciences of the United States of America* vol. 114 12641–12643 (2017).
35. Mesulam, M. M. From sensation to cognition. *Brain* **121 (Pt 6)**, 1013–1052 (1998).
36. Lerner, Y., Honey, C. J., Silbert, L. J. & Hasson, U. Topographic mapping of a hierarchy of temporal receptive windows using a narrated story. *J. Neurosci.* **31**, 2906–2915 (2011).
37. Hasson, U., Nir, Y., Levy, I., Fuhrmann, G. & Malach, R. Intersubject synchronization of cortical activity during natural vision. *Science* **303**, 1634–1640 (2004).
38. Chen, J. *et al.* Shared memories reveal shared structure in neural activity across individuals. *Nat. Neurosci.* **20**, 115–125 (2017).
39. Bhandari, A., Gagne, C. & Badre, D. Just above Chance: Is It Harder to Decode Information from Human Prefrontal Cortex Blood Oxygenation Level-dependent Signals? *J. Cogn. Neurosci.* 1–26 (2018).
40. Mueller, S., Wang, D., Fox, M. D., Yeo, B. & Sepulcre, J. Individual variability in functional connectivity architecture of the human brain. *Neuron* (2013).
41. Gordon, E. M. *et al.* Generation and evaluation of a cortical area parcellation from resting-state correlations. *Cereb. Cortex* **26**, 288–303 (2016).
42. Weiskopf, N., Hutton, C., Josephs, O., Turner, R. & Deichmann, R. Optimized EPI for fMRI studies of the orbitofrontal cortex: compensation of susceptibility-induced gradients in the readout direction. *Magnetic Resonance Materials in Physics, Biology and Medicine* **20**, 39–49 (2007).
43. Glover, G. H. & Law, C. S. Spiral-in/out BOLD fMRI for increased SNR and reduced susceptibility artifacts. *Magn. Reson. Med.* **46**, 515–522 (2001).
44. Birn, R. M., Saad, Z. S. & Bandettini, P. A. Spatial heterogeneity of the nonlinear dynamics in the FMRI BOLD response. *Neuroimage* **14**, 817–826 (2001).
45. Handwerker, D. A., Gonzalez-Castillo, J., D'Esposito, M. & Bandettini, P. A. The continuing challenge of understanding and modeling hemodynamic variation in fMRI. *Neuroimage* **62**, 1017–1023 (2012).
46. Lindquist, M. A., Meng Loh, J., Atlas, L. Y. & Wager, T. D. Modeling the hemodynamic response function in fMRI: efficiency, bias and mis-modeling. *Neuroimage* **45**, S187–98 (2009).
47. Li, Y., Vanni-Mercier, G., Isnard, J., Mauguière, F. & Dreher, J.-C. The neural dynamics of reward value and risk coding in the human orbitofrontal cortex. *Brain* **139**, 1295–1309

(2016).
48. Saez, I. *et al.* Encoding of Multiple Reward-Related Computations in Transient and Sustained High-Frequency Activity in Human OFC. *Curr. Biol.* (2018) doi:10.1016/j.cub.2018.07.045.
49. Lopez-Persem, A. *et al.* Four core properties of the human brain valuation system demonstrated in intracranial signals. *Nat. Neurosci.* **23**, 664–675 (2020).
50. Hill, M. R., Boorman, E. D. & Fried, I. Observational learning computations in neurons of the human anterior cingulate cortex. *Nat. Commun.* **7**, 12722 (2016).
51. Fox, K. C. R. *et al.* Changes in subjective experience elicited by direct stimulation of the human orbitofrontal cortex. *Neurology* **91**, e1519–e1527 (2018).
52. Yih, J., Beam, D. E., Fox, K. C. R. & Parvizi, J. Intensity of affective experience is modulated by magnitude of intracranial electrical stimulation in human orbitofrontal, cingulate and insular cortices. *Soc. Cogn. Affect. Neurosci.* **14**, 339–351 (2019).
53. Hasson, U., Nastase, S. A. & Goldstein, A. Direct Fit to Nature: An Evolutionary Perspective on Biological and Artificial Neural Networks. *Neuron* **105**, 416–434 (2020).
54. Jolly, E. & Chang, L. J. The Flatland Fallacy: Moving Beyond Low–Dimensional Thinking. *Top. Cogn. Sci.* (2019).
55. Sonkusare, S., Breakspear, M. & Guo, C. Naturalistic Stimuli in Neuroscience: Critically Acclaimed. *Trends Cogn. Sci.* **23**, 699–714 (2019).
56. Mukamel, R. *et al.* Coupling between neuronal firing, field potentials, and FMRI in human auditory cortex. *Science* **309**, 951–954 (2005).
57. Honey, C. J. *et al.* Slow cortical dynamics and the accumulation of information over long timescales. *Neuron* **76**, 423–434 (2012).
58. Nastase, S. A., Gazzola, V., Hasson, U. & Keysers, C. Measuring shared responses across subjects using intersubject correlation. *Soc. Cogn. Affect. Neurosci.* **14**, 667–685 (2019).
59. Owen, L. L. W. *et al.* A Gaussian Process Model of Human Electrocorticographic Data. *Cereb. Cortex* **30**, 5333–5345 (2020).
60. Chen, P.-H. *et al.* A Reduced-Dimension fMRI Shared Response Model. in *Advances in Neural Information Processing Systems 28* (eds. Cortes, C., Lawrence, N. D., Lee, D. D., Sugiyama, M. & Garnett, R.) 460–468 (Curran Associates, Inc., 2015).
61. Haxby, J. V., Guntupalli, J. S., Nastase, S. A. & Feilong, M. Hyperalignment: Modeling shared information encoded in idiosyncratic cortical topographies. *Elife* **9**, (2020).
62. Yarkoni, T., Poldrack, R. A., Nichols, T. E., Van Essen, D. C. & Wager, T. D. Large-scale automated synthesis of human functional neuroimaging data. *Nat. Methods* **8**, 665–670 (2011).
63. Manning, J. R., Jacobs, J., Fried, I. & Kahana, M. J. Broadband shifts in local field potential power spectra are correlated with single-neuron spiking in humans. *J. Neurosci.* **29**, 13613–13620 (2009).
64. Chen, G. *et al.* Untangling the relatedness among correlations, part I: Nonparametric approaches to inter-subject correlation analysis at the group level. *Neuroimage* **142**, 248–259 (2016).
65. Haxby, J. V. *et al.* A common, high-dimensional model of the representational space in human ventral temporal cortex. *Neuron* **72**, 404–416 (2011).
66. Vodrahalli, K. *et al.* Mapping between fMRI responses to movies and their natural language annotations. *Neuroimage* **180**, 223–231 (2018).
67. Nir, Y. *et al.* Coupling between neuronal firing rate, gamma LFP, and BOLD fMRI is related to interneuronal correlations. *Curr. Biol.* **17**, 1275–1285 (2007).
68. Keller, C. J. *et al.* Heterogeneous neuronal firing patterns during interictal epileptiform discharges in the human cortex. *Brain* **133**, 1668–1681 (2010).
69. Thomas, J. *et al.* EEG CLassification Via Convolutional Neural Network-Based Interictal Epileptiform Event Detection. *Conf. Proc. IEEE Eng. Med. Biol. Soc.* **2018**, 3148–3151 (2018).

70. Yadav, R., Shah, A. K., Loeb, J. A., Swamy, M. N. S. & Agarwal, R. A novel unsupervised spike sorting algorithm for intracranial EEG. *Conf. Proc. IEEE Eng. Med. Biol. Soc.* **2011**, 7545–7548 (2011).
71. El-Gohary, M., McNames, J. & Elsas, S. User-guided interictal spike detection. *Conf. Proc. IEEE Eng. Med. Biol. Soc.* **2008**, 821–824 (2008).
72. Dümpelmann, M. & Elger, C. E. Visual and automatic investigation of epileptiform spikes in intracranial EEG recordings. *Epilepsia* **40**, 275–285 (1999).
73. Forney, G. D. The viterbi algorithm. *Proc. IEEE* **61**, 268–278 (1973).
74. Kuhn, H. W. The Hungarian method for the assignment problem. *Naval Research Logistics* vol. 52 7–21 (2005).
75. Christoff, K., Irving, Z. C., Fox, K. C. R., Spreng, R. N. & Andrews-Hanna, J. R. Mind-wandering as spontaneous thought: a dynamic framework. *Nat. Rev. Neurosci.* **17**, 718–731 (2016).
76. Reber, J. *et al.* Selective impairment of goal-directed decision-making following lesions to the human ventromedial prefrontal cortex. *Brain* **140**, 1743–1756 (2017).
77. Robinson, M. J. F. & Berridge, K. C. Instant Transformation of Learned Repulsion into Motivational 'Wanting'. *Curr. Biol.* **23**, 282–289 (2013).
78. Isik, A. I. & Vessel, E. A. Continuous ratings of movie watching reveal idiosyncratic dynamics of aesthetic enjoyment. *PLoS One* **14**, e0223896 (2019).
79. Chen, P.-H. A., Jolly, E., Cheong, J. H. & Chang, L. J. Intersubject representational similarity analysis reveals individual variations in affective experience when watching erotic movies. *Neuroimage* **216**, 116851 (2020).
80. Finn, E. S. *et al.* Idiosynchrony: From shared responses to individual differences during naturalistic neuroimaging. *Neuroimage* **215**, 116828 (2020).
81. van Baar, J. M., Chang, L. J. & Sanfey, A. G. The computational and neural substrates of moral strategies in social decision-making. *Nat. Commun.* **10**, 1483 (2019).
82. van Rijckevorsel, K. Cognitive problems related to epilepsy syndromes, especially malignant epilepsies. *Seizure* **15**, 227–234 (2006).
83. Motamedi, G. & Meador, K. Epilepsy and cognition. *Epilepsy Behav.* **4 Suppl 2**, S25–38 (2003).
84. Brunbech, L. & Sabers, A. Effect of Antiepileptic Drugs on Cognitive Function in Individuals with Epilepsy. *Drugs* **62**, 593–604 (2002).
85. Rantanen, K., Eriksson, K. & Nieminen, P. Cognitive impairment in preschool children with epilepsy. *Epilepsia* **52**, 1499–1505 (2011).
86. Elger, C. E., Helmstaedter, C. & Kurthen, M. Chronic epilepsy and cognition. *Lancet Neurol.* **3**, 663–672 (2004).
87. Peirce, J. W. PsychoPy—Psychophysics software in Python. *J. Neurosci. Methods* **162**, 8–13 (2007).
88. Li, G. *et al.* Optimal referencing for stereo-electroencephalographic (SEEG) recordings. *Neuroimage* **183**, 327–335 (2018).
89. Gramfort, A. *et al.* MEG and EEG data analysis with MNE-Python. *Front. Neurosci.* **7**, 267 (2013).
90. Harris, C. R. *et al.* Array programming with NumPy. *Nature* **585**, 357–362 (2020).
91. Virtanen, P. *et al.* SciPy 1.0: fundamental algorithms for scientific computing in Python. *Nat. Methods* **17**, 261–272 (2020).
92. Ossandón, T. *et al.* Transient suppression of broadband gamma power in the default-mode network is correlated with task complexity and subject performance. *J. Neurosci.* **31**, 14521–14530 (2011).
93. Pedregosa, F. *et al.* Scikit-learn: Machine learning in Python. *the Journal of machine Learning research* **12**, 2825–2830 (2011).
94. Kaneshiro, B., Nguyen, D. T., Norcia, A. M., Dmochowski, J. P. & Berger, J. Natural music evokes correlated EEG responses reflecting temporal structure and beat. *Neuroimage* **214**,

116559 (2020).
95. Dmochowski, J. P., Sajda, P., Dias, J. & Parra, L. C. Correlated Components of Ongoing EEG Point to Emotionally Laden Attention – A Possible Marker of Engagement? *Frontiers in Human Neuroscience* vol. 6 (2012).
96. Imhof, M. A., Schmälzle, R., Renner, B. & Schupp, H. T. Strong health messages increase audience brain coupling. *Neuroimage* **216**, 116527 (2020).
97. Maffei, A. Spectrally resolved EEG intersubject correlation reveals distinct cortical oscillatory patterns during free-viewing of affective scenes. *Psychophysiology* **57**, e13652 (2020).
98. Poulsen, A. T., Kamronn, S., Dmochowski, J., Parra, L. C. & Hansen, L. K. EEG in the classroom: Synchronised neural recordings during video presentation. *Sci. Rep.* **7**, 43916 (2017).
99. Thiede, A., Glerean, E., Kujala, T. & Parkkonen, L. Atypical MEG inter-subject correlation during listening to continuous natural speech in dyslexia. *Neuroimage* **216**, 116799 (2020).
100. Chang, W.-T. *et al.* Combined MEG and EEG show reliable patterns of electromagnetic brain activity during natural viewing. *Neuroimage* **114**, 49–56 (2015).
101. Chen, Y. & Farivar, R. Natural scene representations in the gamma band are prototypical across subjects. *Neuroimage* **221**, 117010 (2020).
102. Chang, L., Jolly, E., Cheong, J. H., Burnashev, A. & Chen, A. *cosanlab/nltools: 0.3.11*. (2018). doi:10.5281/zenodo.2229813.
103. Computing, R. & Others. R: A language and environment for statistical computing. *R Core Team* (2013).
104. Chen, P.-H. *et al.* A Reduced-Dimension fMRI Shared Response Model. in *Advances in Neural Information Processing Systems 28* (eds. Cortes, C., Lawrence, N. D., Lee, D. D., Sugiyama, M. & Garnett, R.) 460–468 (Curran Associates, Inc., 2015).
105. Leske, S. & Dalal, S. S. Reducing power line noise in EEG and MEG data via spectrum interpolation. *Neuroimage* **189**, 763–776 (2019).
106. Kooi, K. A. Voltage-time characteristics of spikes and other rapid electroencephalographic transients: semantic and morphological considerations. *Neurology* **16**, 59–66 (1966).
107. Chatrian, G. E., Bergamini, L., Dondey, M. & Klass, D. W. Report on the Committee on Terminology. *Proceedings of the General* (1974).
108. GOTMAN & J. Frequency content of the onset of epileptic seizures. *Electroencephalogr. Clin. Neurophysiol.* **50**, 164–165 (1980).
109. Walczac, T. S. & Jayakar, P. Interictal EEG In Epilepsy: A Comprehensive Textbook, Engel J and Pedley TA eds. (1997).